Turkish Journal of Electrical Engineering and Computer Sciences

Volume 24 | Number 4 Article 61

1-1-2016

An investigation of intelligent controllers based on fuzzy logic and artificial neural network for power system frequency maintenance

NGOCKHOAT NGUYEN

QI HUANG

THI-MAI-PHUONG DAO

Turkish Journal of Electrical Engineering & Computer Sciences

http://journals.tubitak.gov.tr/elektrik/

Research Article

Turk J Elec Eng & Comp Sci
(2016) 24: 2893 – 2909

doi:10.3906/elk-1404-165

An investigation of intelligent controllers based on fuzzy logic and artificial neural network for power system frequency maintenance

NgocKhoat NGUYEN[1,2,*], **Qi HUANG**[1], **Thi-Mai-Phuong DAO**[3,4]

[1]School of Energy Science and Engineering, University of Electronic Science and Technology of China, Chengdu, Sichuan, P.R. China

[2]Faculty of Automation Technology, Electric Power University, Hanoi, Vietnam

[3]College of Electrical and Information Engineering, Hunan University, Changsha, Hunan, P.R. China

[4]Faculty of Electrical Engineering Technology, Hanoi University of Industry, Hanoi, Vietnam

Received: 10.04.2014 • **Accepted/Published Online:** 08.01.2015 • **Final Version:** 15.04.2016

Abstract: In this paper, the design of 3 intelligent control strategies applying fuzzy logic (FL) and artificial neural network (ANN) techniques is investigated to deal with network frequency maintenance against load variations in a large-scale multiarea interconnected power system. These intelligent frequency controllers proposed in this study include FL-PI, ANN-NARMA(nonlinear autoregressive moving average)-L2, and ANN-RMC (reference model control). In principle, they are designed depending upon the tie-line bias control method, which has been applied efficiently for damping frequency oscillations. A mathematical model of an n-control-area interconnected power system with different generation units is built first to apply the control methodologies in order to maintain the grid frequency at its nominal value (50 Hz or 60 Hz). Such a model is considered to be typical candidate of a complicated large-scale power system in reality. Numerical simulation with various cases of load conditions are also implemented in this study using the MATLAB/Simulink package to demonstrate the feasibility and effectiveness of the proposed control strategies. It is found that the 3 intelligent controllers presented in this paper are capable of achieving superiority over the conventional integral regulators in system frequency stabilization. The main dynamic control indexes obtained, especially the overshoot and settling time, are highly promising to effectively extinguish the dynamic responses of the frequency and tie-line power deviations. Thus, the steady state of the power network can be restored more quickly after load variation occurrence. In that way, the stability, reliability, and economy of an electric power grid are able to be guaranteed effectively.

Key words: Large-scale multiarea interconnected power system, load variation, grid frequency deviation, tie-line power change, conventional regulator, intelligent controller

1. Introduction

Together with the output voltage and rotor speed of a synchronous generator, the working frequency in an electric power grid must be maintained at its nominal value (50 Hz or 60 Hz) in order to ensure the stability as well as the reliability of the network. Load in a power system, which mainly depends upon customer demand, is characterized to change randomly and constantly over time. This leads to a power imbalance between the generation and consumption, causing the deviation of the working frequency from the nominal value [1–3]. The occurrence of this deviation will affect power system devices (e.g., motors and transformers), which usually operate directly on the system frequency. The frequency deviation also affects the operation

*Correspondence: khoatnn@epu.edu.vn

of steam turbine blades and active power flows. Therefore, it is necessary to control the network frequency to recover quickly the steady state of the system. The control strategy, especially in a large-scale multiarea interconnected power system, is usually defined as automatic generation control (AGC). The AGC strategy is mainly applied to maintain the network frequency, stabilize and control the energy interchanges between control areas, and keep every generator operating economically. As a crucial part of the AGC scheme, power system frequency maintenance (PSFM) or load-frequency control (LFC) plays an important role to restore the stable operation of a power grid against the load variation. The main objective of the PSFM is to quickly damp the dynamic oscillations of both the network frequency and tie-line power interchange deviations. It means that such deviations must be regulated efficiently to satisfy the desired tolerances in order to bring the steady state back to the grid as quickly as possible after the load variation appearance.

In order to deal with the PSFM problem, conventional integral controllers have been applied initially [2,3]. Due to poor control performances, e.g., high overshoots and long settling times, these regulators must be replaced with improved controllers to achieve an efficient control solution. This leads to the application of modern control techniques such as fuzzy logic (FL) and artificial neural networks (ANNs) to design intelligent control methodologies [4]. A number of studies have been conducted to address this problem. Saravuth et al. in [5] proposed a fuzzy logic controller based on PID to maintain the frequency in a 2-area interconnected power system. Based on the FL technique, the LFC was also presented in [6,7] for a 2-area power network. Shayeghi et al. in [8] investigated the application of ANN based on mu -synthesis to LFC of a 2-area power system. In [9], a wavelet neural network was applied to solve the PSFM in a 2-thermal-thermal interconnected power system. In these reports, the authors only applied either FL or ANNs to deal with the issue of PSFM, and a comprehensive research might not be obtained. Furthermore, a power system with 2 interconnected areas cannot be the typical case of large-scale power networks, which are highly complicated in practice.

The main focus of this study is to design intelligent control methodologies for conducting effectively the LFC in a practical interconnected power grid. For this objective, based on the tie-line bias control strategy, a large-scale n-control-area interconnected power system will be mathematically modeled first. This model, which is designed with various generation units, can be considered as a typical case study of a practical-complicated power system. Using the equivalent replacement method to simplify the modeling process, the proposed model can be applied efficiently for LFC strategies. To apply such a novel model, 3 intelligent controllers based on FL and ANN techniques are investigated to overcome the drawbacks of the conventional integral regulators when dealing with the PSFM problem. These controllers, including FL-PI, ANN-NARMA (nonlinear autoregressive moving average)-L2, and ANN-RMC (reference model control), are able to obtain better control performances. The first controller, FL-PI, is designed depending upon the integration of the FL architecture and PI (proportional-plus-integral) principle. Meanwhile, the 2 remaining methodologies, ANN-NARMA and ANN-RMC, apply the ANN technique to perform the control functionality. Employing such intelligent controllers, especially the novel ANN-RMC architecture, the objectives of the LFC strategy applied to a large-scale power system can be met. The dynamic responses of both the system frequency and tie-line power flow deviations are damped more efficiently to guarantee the stability of the network. An entire evaluation of these controllers along with the conventional integral regulator will be implemented in this work through numerical simulation processes using MATLAB/Simulink software. The model of a 5-control-area interconnected power system with various cases of load conditions is a typical control plant for simulation purposes to demonstrate the feasibility and superiority of the proposed frequency control architectures.

The paper is organized as follows. In Section 2, the tie-line bias control strategy, which can be ap-

plied usefully for designing the load-frequency controllers, will be reviewed briefly. Section 3 then presents a novel method to mathematically model a multi-control-area interconnected power system using the equivalent replacement technique. Subsequently, 3 intelligent controllers will be studied in Section 4 to deal with the PSFM problem. Numerical simulations and discussion are presented in Section 5 to verify the superiority of the proposed control strategies. Finally, the conclusion and future work will be given in the last section of the paper.

2. Tie-line bias control strategy

The network frequency deviation resulting from an energy imbalance between the generation and consumption must be controlled to satisfy an acceptable tolerance. In order to find the solution to this issue, a flat frequency control strategy was used initially. In principle, this technique requires establishing a master machine to maintain the network frequency as its main task. Here, the generation of such a machine should not be significant (from 5% to 10%) compared with that of the remaining machines in the network. This is because it must focus on the essential task of the frequency control [2,3]. Nevertheless, this technique is similar to the centralized control scheme, which is only suitable for a single power system. In fact, a large-scale interconnected power system including a number of generation stations would be consistent with the decentralized control strategies [1]. Additionally, generation areas in such a power system are interconnected by tie-lines for power interchanges. Hence, the deviation of tie-line power flow also needs to be minimized in order to ensure the stability of the scheduled MW demand. This leads to the use of flat tie-line controllers in a large-interconnected power system [2]. When using such controllers, however, they also have to be combined with the flat frequency regulators to make sure that all control objectives of the LFC are satisfied. Moreover, this combination also requires the synchronous operation of regulators, thus making the design of an effective control strategy highly challenging.

A simple and suitable technique that can be applied to adequately solve the PSFM problem in a large-interconnected power system is to use the definition of ACE [3]. This technical term is related to the proportional relationship between the working frequency deviation and tie-line power bias of the area $\#i$ as follows:

$$ACE^i(s) = \Delta P^i_{tie}(s) + B^i.\Delta F^i(s). \tag{1}$$

In Eq. (1), ACE^i, ΔP^i_{tie}, B^i, and ΔF^i are the area control error, tie-line power change, frequency bias factor, and frequency deviation of the ith area, respectively. Our control objective for the PSFM strategy is to concentrate on maintaining the network frequency at its nominal value and tie-line power at the scheduled MW demand as rapidly as possible after the load variations. It means that both the frequency and tie-line power deviations must be extinguished fast enough to obtain the steady state operating condition of the power system. Using the definition of Eq. (1), this control requirement can be achieved when the ACE signal is controlled to satisfy an acceptable tolerance. Moreover, each control area only needs 1 controller to obtain the desired control performances of the PSFM. The LFC implemented in such a manner is typically defined as the tie-line bias control strategy, which will be applied in this work [2–4].

3. Design of an n-control-area interconnected power system model

Let us consider a simple model of an n-control-area interconnected power system as shown in Figure 1a. Assuming that a control area is interconnected through tie-lines to exchange the power demand, this model is able to reach the complexity of a practical power network. In this study, a 5-control-area interconnected power system model (n = 5) indicated in Figure 1b is chosen as a typical case study for simulation purposes to verify

the effectiveness of the LFC strategies. The structure of the *ith* control area is depicted in Figure 2. In Figure 2a, frequency and tie-line sensors are used to collect the data of the network frequency deviation and tie-line power bias, respectively. In the simplest case, each control area consists of 3 main components: a governor, a turbine, and a generator. Turbines with some common types (such as hydraulic, reheat, and nonreheat types) are used to convert the natural energy (e.g., steam or water energy) into mechanical power. Subsequently, synchronous generators are used to convert such power into electric power to deliver to the grid. In a particular case of the PSFM, we only consider the angular rotor speed of a synchronous generator, which is proportional to the network frequency. Finally, governors use signals of the frequency deviations derived from the frequency sensors to handle input flows of the corresponding turbines. Using the nonreheat turbine as a typical case study, transform functions of the above 3 units for control area $\#i$ can be expressed as follows [1–3]:

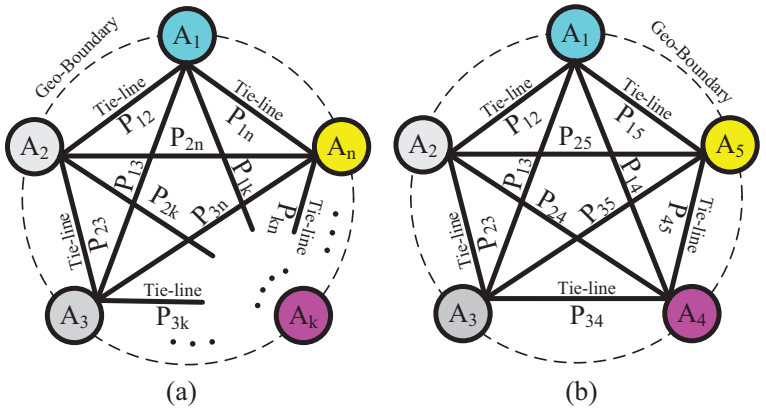

Figure 1. Simple multi-control-area interconnected power system models: (a) n-control-area model, (b) simulation case study (5-control-area model).

(a) for a governor:

$$G_g^i(s) = \frac{1}{1 + s.T_g^i}, \tag{2}$$

(b) for a nonreheat turbine:

$$G_t^i(s) = \frac{1}{1 + s.T_t^i}, \tag{3}$$

(c) for a generator (rotor inertia and load):

$$G_P^i(s) = \frac{K_P^i}{1 + s.T_P^i} = \frac{1}{D^i + s.M^i}. \tag{4}$$

The parameters used in this work can be found in Appendix A.

In practice, each control area includes not only 1 generator but also several generators that are connected in parallel to provide the scheduled power for this area. In addition, there are plenty of governor and turbine units with different types of generation contributions, making the modeling process challenging [1–3]. In this case, it is necessary to simplify the network model by using the equivalent replacement method as given in the following lemma.

Lemma 1 *Given m generators connected in parallel with parameters for the kth generator of inertia constant M_k and load damping factor D_k, such m generators can be replaced with an equivalent generator unit given by the transfer function*

$$G^i_{Peq}(s) = \frac{1}{\sum\limits_{k=1}^{m} \gamma_k.D_k + s.\sum\limits_{k=1}^{m} \gamma_k.M_k} = \frac{1}{D^i_{eq} + s.M^i_{eq}} \tag{5}$$

where γ_k is a rated factor relating to the generation contribution of the kth generator in area $\#i$.

Proof See Appendix C of the paper. □

Using the Lemma given in Eq. (5), the governor and turbine units can also be substituted in the same manner. As a result, a complex generation area as shown in Figure 2b can be replaced efficiently with an equivalent control area. This area includes the parameters, which are similar to a single area. Hence, control area $\#i$ considered as a single area can be used to solve the PSFM problem.

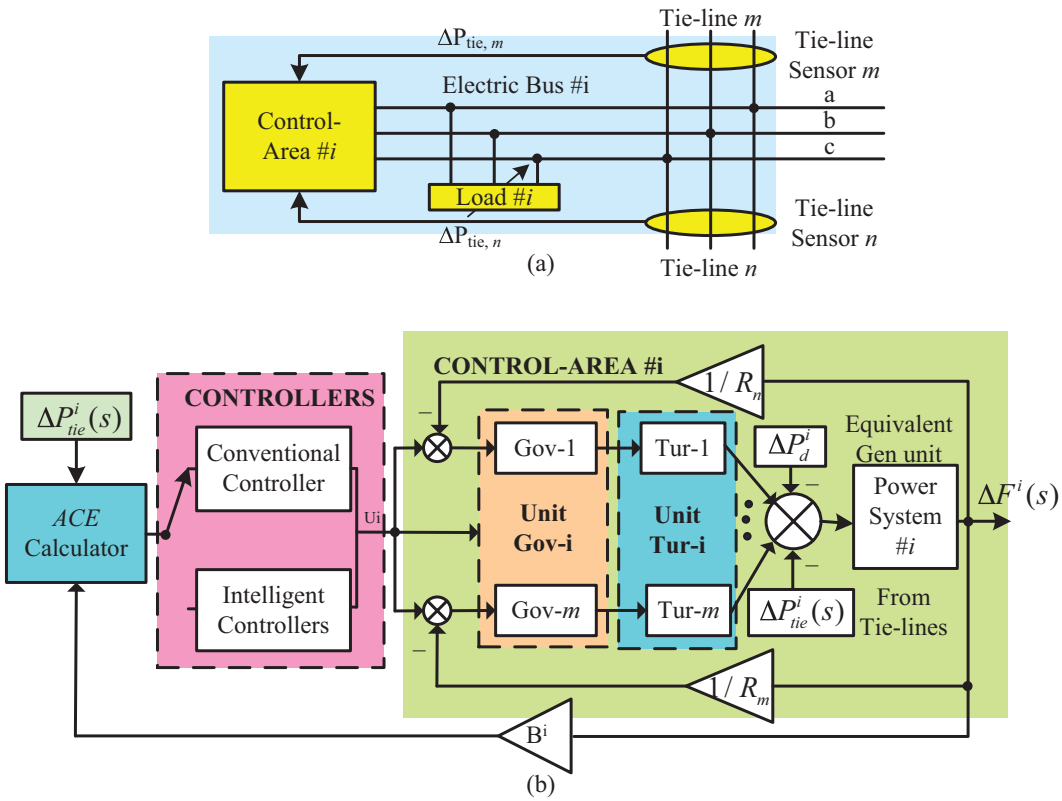

Figure 2. The structure of a control area using different frequency controllers: (a) area $\#i$ with electric bus, (b) area $\#i$ in the *LFC* strategy.

Let us now design a state-space model of an n-control-area interconnected power system after replacing several complicated generation stations with equivalent control areas as mentioned above. Extending the research achievement obtained in [2,3], the mathematical model of the electric power network shown in Figure 1a can be expressed in the Laplace domain as:

$$\Delta F^i(s) = \frac{K^i_P}{1 + s.T^i_P}\left[\Delta P^i_t(s) - \Delta P^i_d(s) - \Delta P^i_{tie}(s)\right], \tag{6}$$

$$\Delta P_t^i(s) = \frac{1}{1+s.T_t^i}\Delta P_g^i(s), \tag{7}$$

$$\Delta P_g^i(s) = \frac{1}{1+s.T_g^i}\left[\Delta P_u^i(s) - \frac{1}{R^i}\Delta F^i(s)\right], \tag{8}$$

$$\Delta P_{tie}^i(s) = \frac{2\pi}{s}\sum_{j=1,j\neq i}^{n} T^{ij}\left[\Delta F^i(s) - \Delta F^j(s)\right], \tag{9}$$

and converting Eqs. (6)–(9) into the time domain, a state-space model can be obtained as follows:

$$\Delta \dot{f}^i(t) = \frac{K_P^i}{T_P^i}\left[-\frac{1}{K_P^i}\Delta f^i(t) + \Delta P_t^i(t) - \Delta P_d^i(t) - \Delta P_{tie}^i(t)\right], \tag{10}$$

$$\Delta \dot{P}_t^i(t) = \frac{1}{T_t^i}\left[-\Delta P_t^i(t) + \Delta P_g^i(t)\right], \tag{11}$$

$$\Delta \dot{P}_g^i(t) = \frac{1}{T_g^i}\left[-\Delta P_g^i(t) + \Delta P_u^i(t) - \frac{1}{R^i}\Delta f^i(t)\right], \tag{12}$$

$$\Delta \dot{P}_{tie}^i(t) = 2\pi\sum_{j=1,j\neq i}^{n} T^{ij}\left[\Delta f^i(t) - \Delta f^j(t)\right]. \tag{13}$$

From Eqs. (10), (11), (12), and (13), a state-space model in matrix form can be established below:

$$\dot{x}(t) = Ax(t) + Bu(t) + F.D \tag{14}$$

$$y(t) = C.x(t) \tag{15}$$

where $x(t)$ is the state variable vector,

$$x(t) = [x_1(t), x_2(t), x_3(t), x_4(t)]^T \tag{16}$$

$$\begin{cases} x_1(t) = \left[\Delta f^1(t), ...\Delta f^i(t), ...\Delta f^n(t)\right]^T \\ x_2(t) = \left[\Delta P_t^1(t), ...\Delta P_t^i(t), ...\Delta P_t^n(t)\right]^T \\ x_3(t) = \left[\Delta P_g^1(t), ...\Delta P_g^i(t), ...\Delta P_g^n(t)\right]^T \\ x_4(t) = \left[\Delta P_{tie}^1(t), ...\Delta P_{tie}^i(t), ...\Delta P_{tie}^n(t)\right]^T \end{cases}$$

$u(t)$ is the input signal vector,

$$u(t) = \left[\Delta P_u^1(t), ...\Delta P_u^i(t), ...\Delta P_u^n(t)\right]^T \tag{17}$$

and D is the load disturbance vector,

$$D = \left[\Delta P_d^1(t), ...\Delta P_d^i(t), ...\Delta P_d^n(t)\right]^T. \tag{18}$$

The state matrix A can be indicated as follows:

$$A = [A_1, A_2, A_3, A_4]^T \tag{19}$$

$$A_1 = \begin{bmatrix} diag\left(\frac{-1}{T_P^1}, ..., \frac{-1}{T_P^n}\right) \\ diag\left(\frac{K_P^1}{T_P^1}, ..., \frac{K_P^n}{T_P^n}\right) \\ zeros(n,n) \\ diag\left(\frac{-K_P^1}{T_P^1}, ..., \frac{-K_P^n}{T_P^n}\right) \end{bmatrix}^T, A_2 = \begin{bmatrix} zeros(n,n) \\ diag\left(\frac{-1}{T_t^1}, ..., \frac{-1}{T_t^n}\right) \\ diag\left(\frac{1}{T_g^1}, ..., \frac{1}{T_g^n}\right) \\ zeros(n,n) \end{bmatrix}^T, A_3 = \begin{bmatrix} diag\left(\frac{-1}{R^1 T_g^1}, ..., \frac{-1}{R^n T_g^n}\right) \\ zeros(n,n) \\ diag\left(\frac{-1}{T_g^1}, ..., \frac{-1}{T_g^n}\right) \\ zeros(n,n) \end{bmatrix}^T,$$

$$A_4 = 2.pi. \begin{bmatrix} \sum_{k=1,k\neq 1}^{n} T^{1k} & -T^{21} & \cdots & -T^{n1} \\ -T^{12} & \sum_{k=1,k\neq 2}^{n} T^{2k} & \cdots & -T^{n2} \\ \vdots & \vdots & \ddots & \vdots \\ -T^{1n} & -T^{2n} & \cdots & \sum_{k=1,k\neq n}^{n} T^{nk} \\ zeros(3n,n) & & & \end{bmatrix}^T.$$

The input and load disturbance matrices are given as:

$$B = \begin{bmatrix} zeros(2n,n) \\ diag\left(\frac{1}{T_g^1}, \cdots, \frac{1}{T_g^n}\right) \\ zeros(n,n) \end{bmatrix}, \text{ and } F = \begin{bmatrix} diag\left(\frac{-K_P^1}{T_P^1}, \cdots, \frac{-K_P^n}{T_P^n}\right) \\ zeros(3n,n) \end{bmatrix}^T \tag{20}$$

where *zeros(m,n)* denotes an $m \times n$ zero matrix, and *diag(*z_1*, ..., *z_n*)* is a diagonal matrix of components z_1, z_2, ..., and z_n.

The output vector $y(t)$ is given below:

$$y(t) = \left[\Delta f^1(t), \cdots, \Delta f^n(t), \Delta P_{tie}^1, \cdots, \Delta P_{tie}^n(t)\right]^T. \tag{21}$$

Finally, the corresponding coefficient matrix of the output vector can be expressed as:

$$C = \begin{bmatrix} I_n & zeros(n,3n) \\ zeros(n,3n) & I_n \end{bmatrix} \tag{22}$$

where I_n is an $n \times n$ identity matrix.

The mathematical model mentioned above can be used efficiently in a number of control strategies for a power system, including the PSFM. In this work, a model of a 5-control-area interconnected power system (n = 5) is selected as a typical case study to apply different controllers for conducting the PSFM strategy. The design of such intelligent load-frequency controllers will be presented in the following section.

4. Intelligent controllers based on the tie-line bias control strategy

4.1. Fuzzy logic-based controller

Recently, the fuzzy logic technique has made great achievements in industrial control systems. Controllers based on the FL technique can operate effectively without enough parameters of a control plant. This means that such controllers only depend on the knowledge of experts through the logic rule bases [10–13]. Therefore, these FL controllers have been applied more widely and usefully in complex control systems, including large-scale power systems, to solve the PSFM problem.

Let us consider an FL controller which is used for the ith control area as shown in Figure 3. Such an FL architecture (illustrated in Figure 3) uses 2 input signals, *ace* and its derivative *dace*, relating to ACE and $dACE$ as follows:

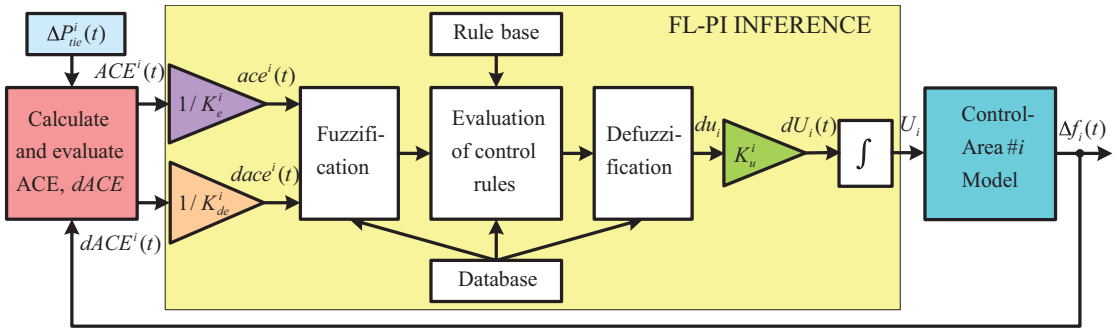

Figure 3. The structure of a fuzzy logic controller for control area $\#i$.

$$ace^i(t) = \frac{1}{K^i_e} ACE^i(t) = \frac{1}{K^i_e}\left(\Delta P^i_{tie}(t) + B^i \Delta f^i(t)\right) \tag{23}$$

$$dace^i(t) = \frac{1}{K^i_{de}} \frac{d}{dt} ACE^i(t) = \frac{1}{K^i_{de}} \frac{d}{dt}\left(\Delta P^i_{tie}(t) + B^i \Delta f^i(t)\right) \tag{24}$$

where K^i_e and K^i_{de} are the scaling coefficients corresponding to ACE^i and its derivative $dACE^i$, respectively. In general, the principle of an FL inference can be expressed as:

$$du^i(t) = K_1.ace^i(t) + K_2.dace^i(t) \tag{25}$$

where K_1 and K_2 are internal gain factors of the FL reasoning. From Eqs. (23)–(25), one can be obtained as below:

$$U^i(t) = K^i_u.u^i(t) = K^i_u. \int u^i(t)dt = K^i_u \left[\frac{K_1}{K^i_e} \int ACE^i(t)dt + \frac{K_2}{K^i_{de}}.ACE^i(t)\right] \tag{26}$$

thus,

$$U^i(t) = K_P.ACE^i(t) + K_I. \int ACE^i(t)dt. \tag{27}$$

Here, $K_P = K_2.K^i_u/K^i_{de}$ and $K_I = K_1.K^i_u/K^i_e$ respectively denote 2 factors, which are highly similar to the proportional and integral coefficients of a PI regulator. As a result, the proposed FL controller shown in Figure 3 is able to be categorized as the PI-type FL model (FL-PI) [6,14]. To implement such an inference, there are

totally 49 rules used in this work as represented in Table 1. Here, each of 2 inputs employs 7 logic levels of NB, NM, NS, ZE, PS, PM, and PB, which stand for negative big, negative medium, negative small, zero, positive small, positive medium, and positive big, respectively. Meanwhile, the output of the FL architecture uses 9 linguistic terms, including NB (negative big), NM (negative medium), NS (negative small), NVS (negative very small), ZE (zero), PVS (positive very small), PS (positive small), PM (positive medium), and PB (positive big). Each rule indicated in Table 1 can be written as: "IF the first input $ace(t)$ is $\boldsymbol{e}$ and the second input $dace(t)$ is $\boldsymbol{de}$ THEN the output $u(t)$ is $\boldsymbol{u}$". For example, the last rule (corresponding to the last row and the last column of Table 1) is: "IF $ace(t)$ is **PB** and the second input $dace(t)$ is **PB** THEN the output $u(t)$ is **PB**". According to the composition rule theory of the FL model, each given rule can be used to perform a meaningful control action in accordance with a specific condition of the variables. Such a composition rule, employed for the FL inference to generate the output control signal, should be chosen properly to achieve the desired control quality. For this study, the MAX-MIN (maximum-minimum) composition is selected since it is the most common and efficient composition for the FL inference. According to such a composition rule, the output membership function is calculated by a MIN operator, whereas the combined fuzzy output will be given by a MAX mechanism.

Table 1. Rule matrix for the proposed FL controller.

dace(t)	*ace(t)*						
	NB	NM	NS	ZE	PS	PM	PB
NB	NB	NB	NB	NM	NS	NVS	ZE
NM	NB	NB	NM	NS	NVS	ZE	PVS
NS	NB	NM	NS	NVS	ZE	PVS	PS
ZE	NM	NS	NVS	ZE	PVS	PS	PM
PS	NS	NVS	ZE	PVS	PS	PM	PB
PM	NVS	ZE	PVS	PS	PM	PB	PB
PB	ZE	PVS	PS	PM	PB	PB	PB

Table 2. Parameters for the proposed ANN-based controllers.

Parameters	ANN-NARMA-L2	ANN-RMC	
		ANN Controller	Plant Model
Size of hidden layer	13	13	10
Sampling internal (s)	0.1	0.05	0.05
No. delayed ref. inputs	N/A	2	N/A
No. delayed plant inputs	3	N/A	2
No. delayed plant outputs	2	3	2
No. delayed cont. outputs	N/A	2	N/A
Training samples	5000	5000	5000
Training epochs	150	10	30
Training function	trainlm	trainlm	trainlm
Trained error	10^{-5}	10^{-4}	10^{-4}

4.2. ANN-NARMA-L2-based controller

Together with the FL technique, ANNs have been applied widely and usefully to replace the conventional controllers using integral, PI, or PID regulators in a number of complex control systems. The concept of the ANN was defined in an attempt to imitate the intelligent function of the human brain to solve control problems

requiring technical criteria of high quality [15,16]. Similar to a human brain, an ANN has a parallel natural structure, leading to the capability to operate in real time more rapidly and effectively. Additionally, because of the off-line training ability, multilayer ANNs can be built with small computation time for designing approximate models to deal with the feedforward control strategies. Consequently, ANN-based control techniques can also be applied in several suitable controllers to solve the PSFM problem.

In this section, the design of an ANN-NARMA-L2 controller is presented first. Let us now recall the state space model of an n-control-area power system expressed in Eqs. (14) and (15) in the absence of load perturbation:

$$\dot{x}(t) = Ax(t) + Bu(t), \tag{28}$$

$$y(t) = C.x(t). \tag{29}$$

From Eqs. (28) and (29), it is easy to design the discrete model as indicated below:

$$x[k+1] = A.x[k] + B.u[k] = f(x[k], u[k]), \tag{30}$$

$$y[k] = C.x[k]. \tag{31}$$

According to the literature [17,18], the above model can be defined as a NARMA (nonlinear autoregressive moving average) with the following output:

$$y[k+d] = F(y[k], y[k-1], ...y[k-n+1], u[k], u[k-1], ...u[k-m+1]), \tag{32}$$

where d, m, and n denote the relative order, input, and output delays, respectively. For the control objective, the output $y[k+d]$ must be treated to follow the reference value $y_{ref}[k+d]$. In order to achieve efficient control features, a NARMA-L2 model should be applied [16–18]. In principle, the algorithm of a NARMA-L2 model is based on the removal of nonlinear elements of the given system to generate an approximately linear system. In this case, the output signal of a NARMA-L2 controller can be computed as:

$$u[k+1] = \frac{y_{ref}[k+d] - h\left(y[k], y[k-1], ...y[k-n+1], u[k], u[k-1], ...u[k-m+1]\right)}{g\left(y[k], y[k-1], ...y[k-n+1], u[k], u[k-1], ...u[k-m+1]\right)}. \tag{33}$$

Each model proposed above uses 2 multilayer ANNs to obtain the approximate computation of 2 functions, $h(\cdot)$ and $g(\cdot)$. The detailed structure of an ANN-NARMA-L2 model employed for control area $\#i$ is represented in Figure 4. In this study, each ANN composed of a 9-neuron hidden layer will be trained off-line using 5000 samples and 0.01 (s) sampling interval. Moreover, a 3-delayed plant input (m = 3) and a 2-delayed plant output (n = 2) are used to feed the neural network plant model. A training process will also be implemented to meet the acceptable errors. In conclusion, there are a total of such n ANN-NARMA-L2 architectures used for designing the LFC controllers.

4.3. ANN-RMC-based controller

The second ANN model used in this work to achieve the optimal control performances is defined as ANN-RMC [16]. The principle of this control strategy is presented in Figure 5. In each model, 2 neural networks are used for the ith control area, including an ANN-controller and ANN-identification plant. The inputs of the ANN-controller are similar to the ANN-NARMA-L2 controllers as mentioned above. On the other hand, the

second neural network applied to identify the corresponding control area uses the output of the first network $u(k)$ as its input. In addition, a reference area model is also used in this control architecture to evaluate the error of its output and the real ACE in order to train the ANN-controller. Thus, the ANN-controller is trained along with the ith control-area model to track the corresponding reference model. This control strategy is typically defined as a direct ANN-RMC scheme since the generated error will be propagated backwards through the controller.

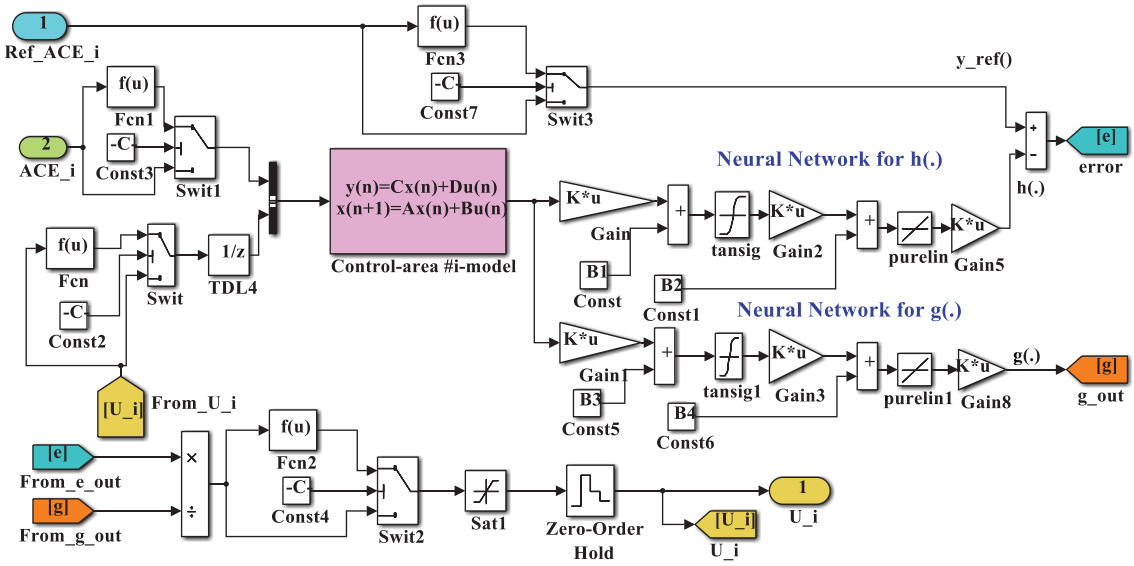

Figure 4. The architecture of an ANN-NARMA-L2 model.

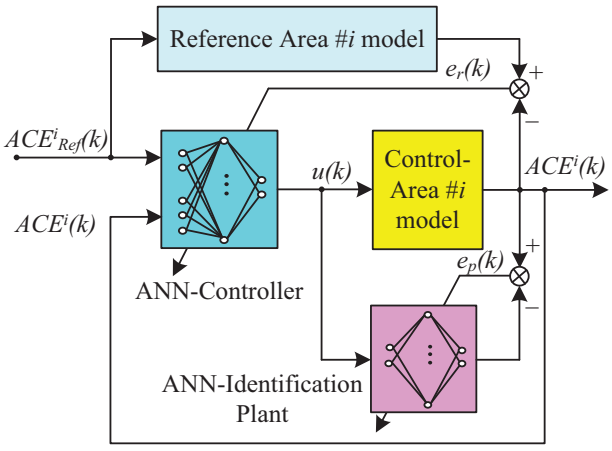

Figure 5. The control structure of an ANN-RMC model.

To implement the control scheme, control area $\#i$ is identified first to imitate the forward model of the control plant. In this work, we use the ANN-identification model with a 2-10-2 architecture to achieve a desired training error ($\varepsilon = 0.01\%$). Also, a 5-13-2 architecture is designed for each ANN-controller to obtain the similar training error. The parameters of the proposed control strategy are indicated in Table 2.

After training, the ANN-identification plant is then embedded in the control system to integrate with the ANN-controller. Consequently, the ANN-controller is trained more effectively through the ANN-identification model in order to achieve the desired control characteristics. The accuracy of these control properties depends

on the choice of a suitable reference area model. In this work, a proper model with the necessary parameters ($T_g = 0.08$, $T_t = 0.3$, $K_P = 5$, $T_P = 18$, and $1/R = 0.35$) has been chosen. Simulation processes will be implemented in the next section to verify the superiority of the proposed control architectures.

5. Numerical simulation and discussion

In this section, MATLAB/Simulink package version 2013a will be employed to perform numerical simulation processes in order to demonstrate the feasibility and superiority of the proposed control strategies. The 5-control-area interconnected power system model shown in Figure 1b is selected as a typical case study of the large-complicated electric grids in reality. Due to the variety and complexity of the practical load variations, 2 simulation cases considered in this study are as follows:

1. In the first simulation case, load variation is only assumed to appear in the first area assuming that there are no load variations in the other areas for this case.
2. In the second simulation case, load variations with different magnitudes and starting times are fed to all 5 control areas. This case would be highly close to a practical condition of the load changes in a power system.

The simulation parameters used for the power system model with the above 2 load variation cases are described specifically in Appendix B. Based on the tie-line bias control strategy and the modeling method of an interconnected power system mentioned earlier, the simulation model can be built in the Simulink environment as shown in Figure 6. Here, 3 intelligent controllers (FL-PI, ANN-NARMA-L2, and ANN-RMC) as well as the conventional integral regulator are applied to maintain the system frequency against load variations. The control performances of these controllers will be evaluated depending upon the simulation results obtained as a typical case study to verify the superiority of the proposed control methodology.

In order to effectively realize the PSFM strategy, the output vector $y_{FP} = [\Delta f^i, \Delta P^i_{tie}]^T$ has to converge towards the zero-steady state $y^0_{FP} = [zeros(1,n), zeros(1,n)]^T$ with the best dynamic characteristics, such as the smallest overshoot and shortest settling time. Hence, these control performance indexes are used to assess the effectiveness of all 4 controllers for stabilizing the system frequency.

Simulation results obtained for the first case are shown in Figures 7–9. Meanwhile, Figures 10 and 11 and Tables 3 and 4 represent several results for the second simulation case. In the first simulation case, the dynamic oscillations of the network frequency deviations in 2 areas (the first and fifth control areas) resulting from 4 controllers are plotted in Figure 7. The frequency change responses in the control-area #4 are described in Figures 8a and 8b. As shown in Figure 8b, the frequency errors between pairs of controllers, including the conventional integral and each of 3 intelligent regulators, are calculated to represent the better dynamic performances of the proposed control strategies. Given a desirable frequency tolerance of 0.1%, 2 important control indexes, namely the overshoot and settling time, are also computed for all control areas as presented in Figure 9. From these results, it is easy to deduce several conclusions as follows.

1. When load variation occurs in a certain area (e.g., the first area in this case), such an area is subjected to the worst impact (the highest overshoots or maximum peaks and the longest settling times).
2. All 3 intelligent controllers proposed in this study are able to achieve better control performances in comparison with the conventional integral regulator when solving the PSFM issue. Both the overshoot

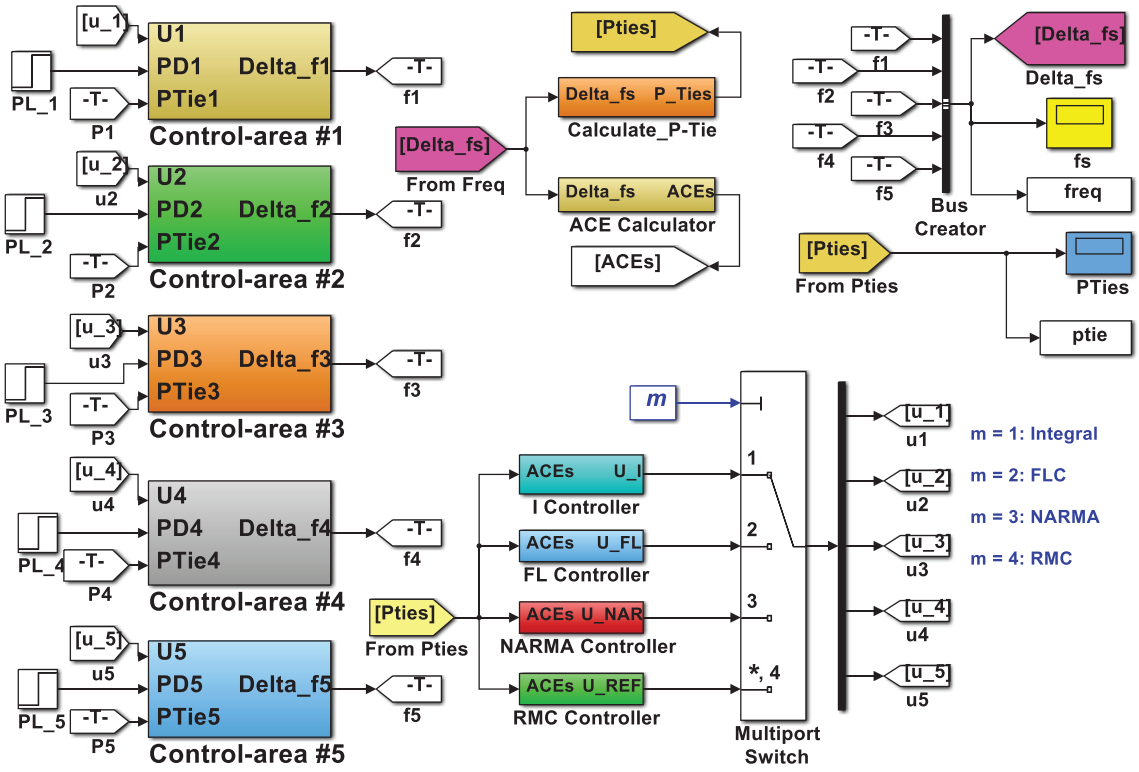

Figure 6. A 5-control-area interconnected power system model built in the MATLAB/Simulink environment.

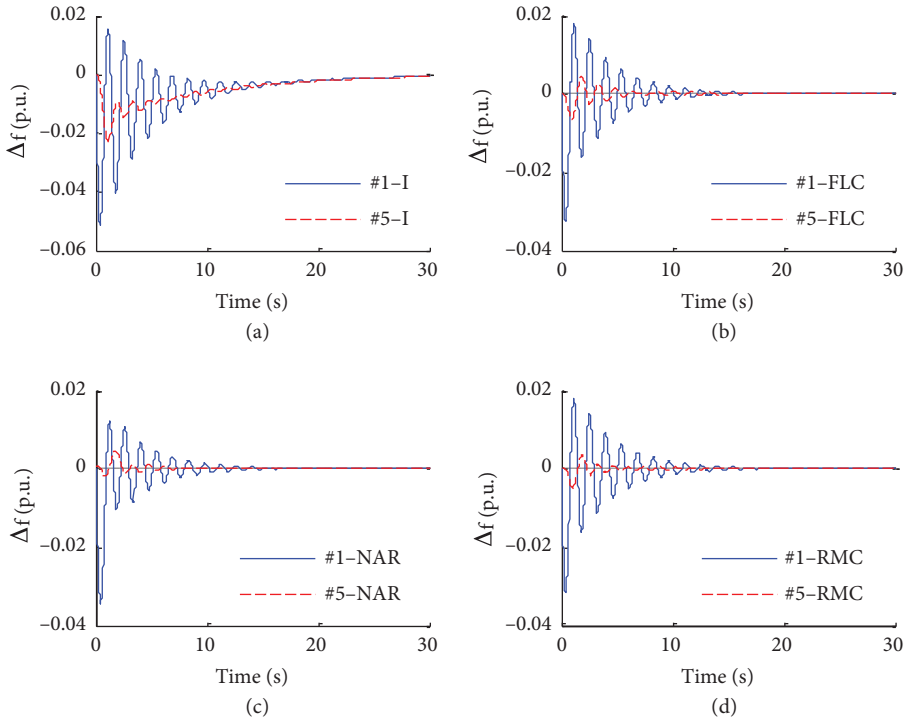

Figure 7. Frequency deviations of area #1 and area #5 for the first simulation case.

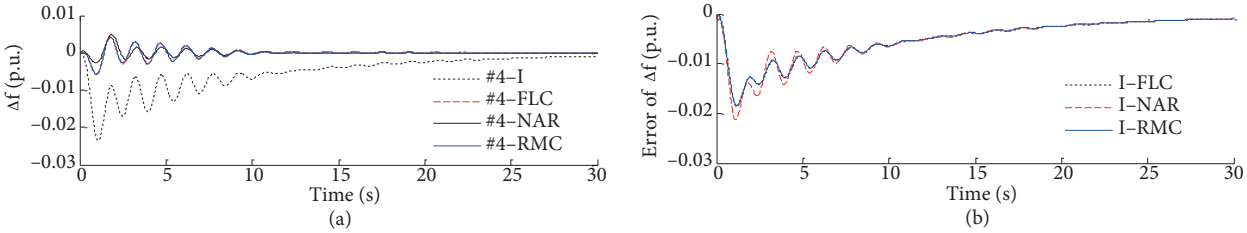

Figure 8. The dynamic response of the frequency change for area #4 in the first simulation case.

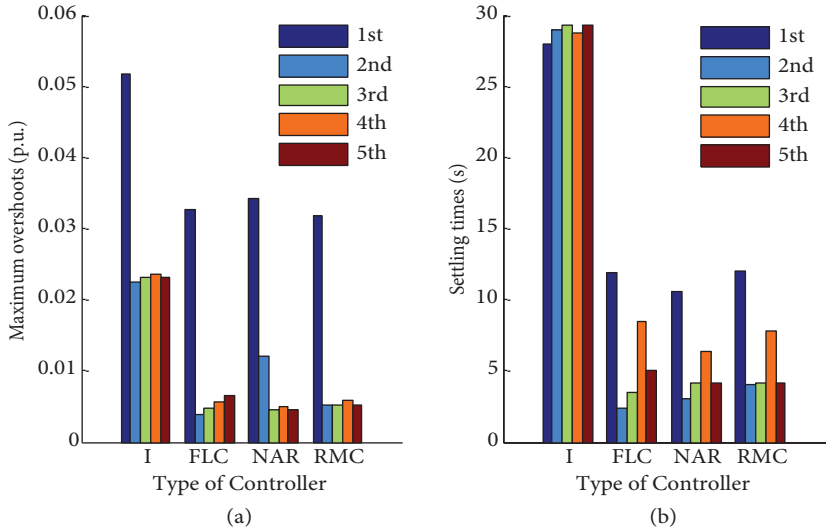

Figure 9. A numerical comparison for 4 control methodologies in the first case: (a) overshoots, (b) settling times.

and settling time indexes obtained by using such intelligent controllers are much smaller than those of the integral regulator (see Figure 9).

3. With the better control performances obtained, a large-interconnected power system applying these intelligent controllers can operate more efficiently and reliably in practical load conditions. The dynamic oscillation of the network frequency deviation is damped fast enough to satisfy a desired tolerance (see Figures 7 and 8). As a result, it can be said that such an electric power grid is able to quickly restore the steady-state operating condition after the load variation, ensuring the stability of the network.

4. The superiority of all 3 intelligent controllers would be evaluated efficiently and equally through the simulation results obtained (see Figures 7–9). Therefore, each of them can feasibly substitute for the conventional integral controller to protect the grid frequency against the load variations.

The above conclusions can also be verified through simulation results obtained in the second case. Figure 10 shows the frequency deviation responses in area #2 and area #4. Figure 11 describes a numerical comparison regarding the overshoots and settling times of 4 controllers in all control areas. It is found that when load variations appear in all areas, the power network will be subjected to the worse influences. The main control performances in this case, such as the overshoots and settling times, are worse than those of the first simulation case (see Figures 9 and 11). Furthermore, once the load variation occurs randomly in an area, the frequency

deviation will increase immediately. Hence, the control strategy must respond quickly enough to effectively extinguish such a frequency oscillation. It can be said that the control methodology applying 3 intelligent controllers proposed in this study is capable of achieving this performance. Simulation results obtained (shown in Figures 10 and 11) can be used for demonstration purposes. To attain an entire assessment, Tables 3 and 4 numerically indicate several comparisons of 3 intelligent controllers with the conventional regulator for both the frequency and tie-line power deviations. According to Table 3, both maximum overshoot and settling time of 3 intelligent controllers are better than those of the conventional integral regulator. All comparison results are much smaller than 100%, leading to the outperformance of the proposed intelligent controllers. Similarly, better results in terms of the tie-line power flow deviations can be found in Table 4 for this case. Obviously, all of these results, in spite of the typical case studies, are able to demonstrate the effectiveness, superiority, and feasibility of the proposed intelligent control methodology. Thus, they are capable of perfectly replacing the integral regulators when solving the network frequency maintenance problem.

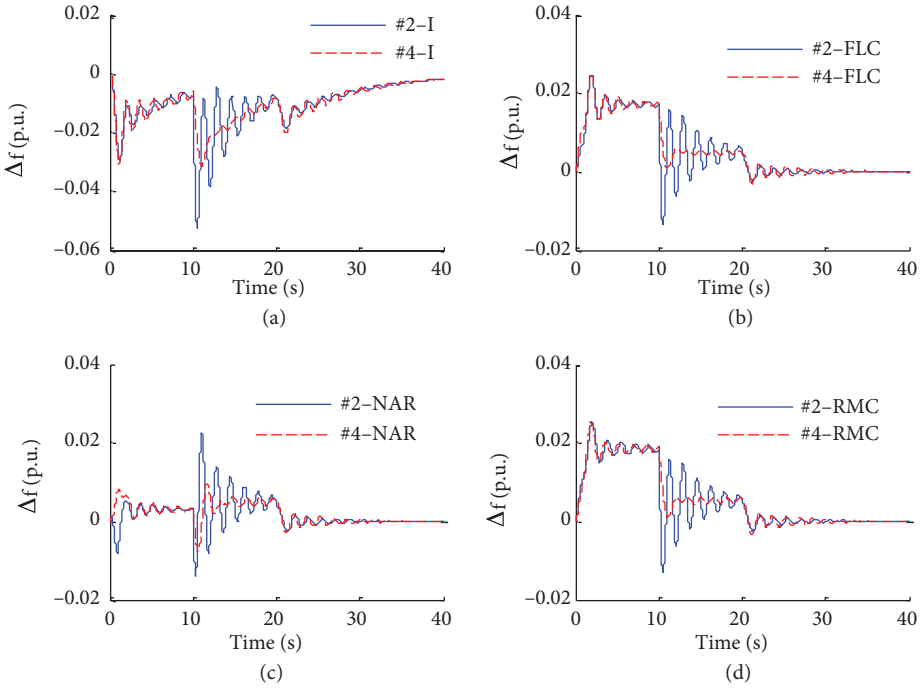

Figure 10. Frequency changes of areas #2 and #4 in the second simulation case.

Table 3. The comparison (%) of the maximum overshoots and settling times with the desirable frequency tolerance of 0.1% for the second simulation case.

Control area		Maximum overshoots			Settling times		
		FLC-I	NAR-I	RMC-I	FLC-I	NAR-I	RMC-I
Frequency deviation	Area #1	71.5636	62.2322	72.5691	47.6720	47.6504	47.7585
	Area #2	47.5435	42.9691	48.2838	50.0491	51.8212	50.1788
	Area #3	77.2462	39.8132	85.4418	59.8411	60.2469	60.3110
	Area #4	79.1588	30.9965	81.2192	56.8913	56.9565	58.5652
	Area #5	60.5207	30.8249	62.8242	64.5000	66.6111	66.5652

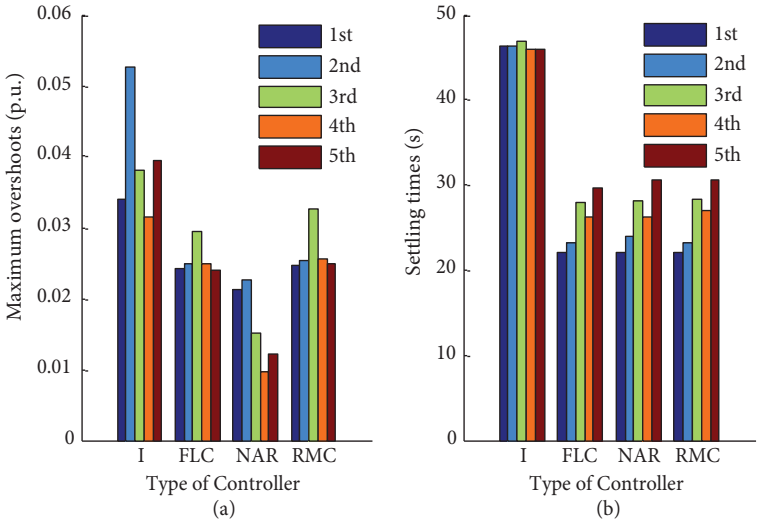

Figure 11. A numerical comparison of 4 controllers for the second simulation case: (a) overshoots, (b) settling times.

Table 4. A numerical comparison of tie-line power deviations for the second simulation case.

Control area		Maximum overshoots (p.u.)				Comparison (%)		
		I	FLC	NAR	RMC	FLC-I	NAR-I	RMC-I
Tie-line power deviation	Area #1	0.0083	0.0038	0.0020	0.0017	45.5473	24.3712	20.0810
	Area #2	0.0204	0.0038	0.0041	0.0036	18.6660	20.0706	17.4168
	Area #3	0.0157	0.0024	0.0062	0.0034	15.4838	39.2616	21.8867
	Area #4	0.0077	0.0025	0.0035	0.0017	31.8774	46.1453	22.5292
	Area #5	0.0102	0.0035	0.0040	0.0028	34.3907	39.6616	27.8803

6. Conclusion and future work

The main contribution of this paper is to investigate intelligent control strategies applying the FL and ANN techniques to deal with the frequency stabilization against load variations in a large-scale multi-control-area interconnected power system. One of the new contributions is to focus on designing an n-control-area interconnected power system model based on the tie-line bias control method, which is highly significant to testify to the effectiveness and feasibility of a load-frequency controller. Furthermore, the ANN-RMC regulator, 1 of 3 intelligent controllers proposed in this study, is another new contribution to design an efficient control methodology for stabilizing the network frequency. All 3 intelligent controllers proposed (FL-PI, ANN-NARMA-L2, and ANN-RMC) are able to quickly and efficiently damp the dynamic oscillations of the system frequency and tie-line power flow deviations, and hence ensure the stability of an electric grid against the load variations. The evaluations resulting from the simulation processes for 2 typical cases with various load variation conditions have validated the superiority of the proposed control strategies over the conventional integral regulators. Computational statistical analyses revealing the capability for the practical applications of these intelligent controllers have also been realized in this study. Each of the 3 controllers can be selected as an efficient candidate to solve the PSFM problem in reality.

For future work, in order to enhance the adaptability and practical application of the proposed control architectures, a large-scale electric power grid with nonlinearities and uncertainties should be considered, such as the Sichuan power system in China. The coordination obtained from some pairs of the proposed intelligent controllers may also be studied to utilize the dominant advantages of each regulator, improving further the

superiority of the load-frequency control scheme. In addition, the 3 intelligent controllers proposed should be integrated with biologically inspired metaheuristic techniques (e.g., genetic algorithm and particle swarm optimization) in order to design the adaptive control methodologies for a practical power network.

Acknowledgment

This work was supported by the Natural Science Foundation of China (NSFC, Grant No. 51277022). The authors would like to thank Dr Wahid, Dr Stephen, and Dr Gustav for their help to check the English grammar of the paper.

References

[1] Wen T, Hong Z. Robust analysis of decentralized load frequency control for multi-area power systems. Int J Elec Power 2012; 43: 996-1005.

[2] Murty PSR. Operation and Control in Power Systems. Hyderabad, India: BS Publications, 2008.

[3] Kundur P. Power System Stability and Control. New York, NY, USA: McGraw-Hill, 1994.

[4] Shashi KP, Soumya RM, Nand K. A literature survey on load-frequency control for conventional and distribution generation power systems. Renew Sust Energ Rev 2013; 25: 318-334.

[5] Saravuth P, Issarachai N. Optimal fuzzy logic-based PID controller for load–frequency control including superconducting magnetic energy storage units. Energ Convers Manage 2008; 49: 2833-2838.

[6] IIhan K, Ertugrul C. Fuzzy logic controller in interconnected electrical power systems for load-frequency control. Int J Elec Power 2005; 27: 542-549.

[7] Ali MY, Ayman AA. Effect of non-linearities in fuzzy approach for control a two-area interconnected power system. In: IEEE 2010 International Conference on Mechatronics and Automation; 4–7 August 2010; Xi'an, China. pp. 706-711.

[8] Shayeghi H, Shayanfar HA. Application of ANN technique based on *mu* -synthesis to load frequency control of interconnected power system. Int J Elec Power 2006; 28: 503-511.

[9] Hemeida AM. Wavelet neural network load frequency controller. Energ Convers Manage 2005; 46: 1613-1630.

[10] Mohammad AH, Abbas K, Mohammad J. Fuzzy based load frequency controller for multi area power system. Tech J Engin App Sci 2013; 3: 3433-3450.

[11] Rajani KM, Nikhil RP. A robust self-tuning scheme for PI- and PD- type fuzzy controllers. IEEE T Fuzzy Syst 1999; 7: 2-16.

[12] Hassan MAM, Malik OP. Implementation and laboratory test results for a fuzzy logic self-tuned power system stabilizer. IEEE T Energy Conver 1993; 8: 221-228.

[13] Chandrakala KRMV, Balamurugan S, Sankaranarayanan K. Variable structure fuzzy gain scheduling based load frequency controller for multi source multi area hydro thermal system. Int J Elec Power 2013; 53: 375-381.

[14] Bimal KB. Modern Power Electronics and AC Drives. Upper Saddle River, NJ, USA: Prentice Hall, 2002.

[15] Kumpati SN, Snehasis M. Adaptive control using neural networks and approximate models. IEEE T Neural Networ 1997; 8: 475-485.

[16] Haykin S. Neural Networks: A Comprehensive Foundation. New York, NY, USA: MacMillan, 1994.

[17] Adetona O, Sathananthan S, Keel LH. Robust adaptive control of nonaffine nonlinear plants with small input signal changes. IEEE T Neural Networ 2004; 15: 408-416.

[18] Zhi L, Yun Z. Adaptive control design of neural fuzzy system for NARMA-L2 model. In: 2006 Proceedings of the 6th World Congress on Intelligent Control and Automation; 21–23 June 2006; Dalian, China. pp. 2801-2805.

A. Appendix

Nomenclature

i index of control area $\#i$, $i = 1, 2, \ldots$ n

f network frequency, Hz

$\Delta f^i(t)$ network frequency deviation, in time domain, p.u.

$\Delta F^i\ (s)$ network frequency deviation, in Laplace domain, p.u.

ACE^i Area control error

U^i control signal for the ith control area

ΔP_d^i load variation, p.u.

ΔP_{tie}^i tie-line power flow deviation, p.u.

T_g^i time constant of governor, s

T_t^i time constant of nonreheat turbine unit, s

D^i load damping factor, p.u. MW/Hz

M^i generator inertia constant, p.u.

K_P^i gain of power system, Hz/p.u.MW

T_P^i time constant of power system, s

T^{ij} tie-line time constant, s

B^i frequency bias factor, MW/p.u.Hz

R^i speed regulation, Hz/MW

G_g^i transfr function of the governor unit

G_t^i transfer function of the nonreheat turbine unit

G_P^i transfer function of the rotor inertia and load (power system)

B. Appendix

The 5-control-area interconnected power system model parameters.

$$T_g^1 = 0.08, T_g^2 = 0.12, T_g^3 = T_g^4 = T_g^5 = 0.1; T_t^1 = 0.3, T_t^2 = 0.3, T_t^3 = T_t^4 = T_t^5 = 0.35;$$

$K_P^1 = 120, K_P^2 = 100, K_P^3 = K_P^4 = K_P^5 = 98; T_P^1 = 18, T_P^2 = 20, T_P^3 = T_P^4 = T_P^5 = 25; T^{ij} = 0.0707;$ the first simulation case: $\Delta P_D = [2\%, 0, 0, 0, 0]^T$ at starting time: 0 (s); the second simulation case: $\Delta P_D = [1\%, 2\%, 1.5\%, 0.5\%, 1\%]^T$ at starting times: 0 (s), 10(s), 0(s), 10(s), and 0(s), respectively.

C. Appendix

Proof of the lemma given in Eq. (5).

To prove the lemma, the finite induction method can be used due to the limit of generators in each practical generation area. Assume that 2 generators are interconnected in parallel with the corresponding transfer functions

$$G_{P1}(s) = \frac{1}{D_1 + s.M_1}, G_{P2}(s) = \frac{1}{D_2 + s.M_2}$$

and 2 rated powers P_1 and P_2.

The corresponding addition function of such 2 generators and the equivalent transfer function according to the lemma of Eq. (5) can be given as

$$G(s) = \gamma_1 G_{P1}(s) + \gamma_2 G_{P2}(s) = \gamma_1 \frac{1}{D_1 + s.M_1} + \gamma_2 \frac{1}{D_2 + s.M_2},$$

$$G_{eq}(s) = \frac{1}{(\gamma_1 D_1 + \gamma_2 D_2) + s\,(\gamma_1 M_1 + \gamma_2 M_2)}$$

where $\gamma_1 = \frac{P_1}{P_1+P_2} and \gamma_2 = 1 - \gamma_1$. Using Bode and Nyquist analysis methods, it is easy to prove that the dynamic responses of both transfer functions $G(s)$ and $G_{eq}(s)$ are very close. Let us now consider an example with $D_1 = 0.02$, $M_1 = 0.2$, $D_2 = 0.018$, $M_2 = 0.15$, $P_1 = 125$ MW, and $P_2 = 375$ MW. The transfer functions, $G(s)$ and $G_{eq}(s)$, can be calculated as follows:

$$G(s) = \frac{1}{0.03s^2 + 0.0066s + 0.00036} \text{ and } G_{eq}(s) = \frac{1}{0.1625s + 0.0185}.$$

Both Bode and Nyquist diagrams of such 2 transfer functions are very close (see Figure 12). This leads clearly to the proof of the given lemma.

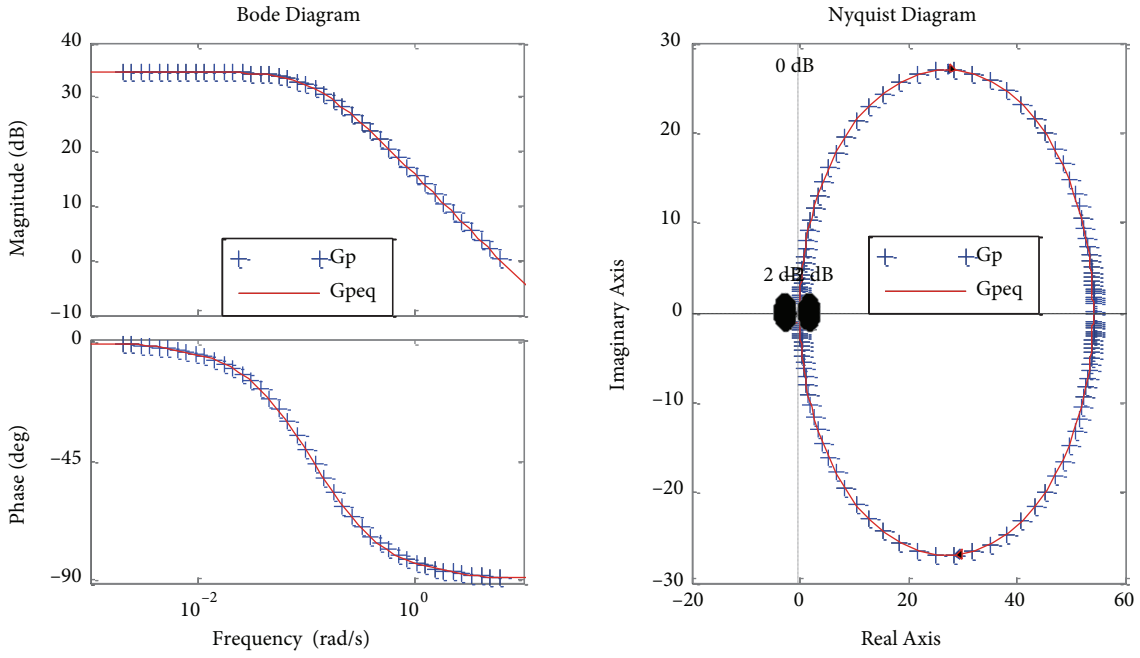

Figure 12. An illustration for proof of the lemma given in Eq. (5).